ADVANCED INTELLIGENT SYSTEMS
Open Access
www.advintellsyst.com

Electrical Tissue Adhesives for Strain-Insensitive In-situ Biosensing

Tsz Hung Wong, Jiabin Liu, Yijie Cheng, Yilin Xie, Camryn Anway, Ruihao Lu, Chuwei Ye, Zhaohan Yu, Yuan Wang, Xinyue Liu, and Shaoting Lin**

In-situ biosensing, a rapidly evolving field that focuses on the development of biosensors capable of on-site detection of biomolecules directly from local tissue regions, holds the potential to revolutionize medicine through real-time monitoring, personalized diagnosis, and targeted therapies. However, interfacing rigid, nonstretchable biosensors with soft, deformable tissues presents significant challenges due to their fundamentally contradictory properties. Herein, an electrical tissue adhesive featuring an entangled adhesive polymer network interpenetrated with a sacrificial dissipative polymer network is developed, which can rapidly and robustly adhere electrochemical biosensors with biological tissues, enabling strain-insensitive physiological monitoring. The electrical tissue adhesive achieves a high fracture toughness of up to 3000 J m^{-2}, a low Young's modulus of around 20 kPa, superior stretchability up to 15 times its initial length, and an overall biosensor-tissue interfacial toughness of up to 500 J m^{-2}. Using an electrochemical glucose sensor as one example, it is demonstrated that the electrical tissue adhesive can maintain resilient glucose sensing under various stress states and stretch levels. Additionally, the application of the electrical tissue adhesive for in-situ monitoring of exercise and diet in subjects with various BMIs is demonstrated by measuring glucose concentration in sweat.

1. Introduction

In-situ biosensing, a rapidly evolving field that focuses on the development of biosensors capable of on-site detection of biomolecules directly from local tissue regions, holds great promise for revolutionizing the field of medicine. Compared to existing sensing techniques such as enzyme-linked immunosorbent assay and home-screening tests, in-situ biosensing offers superior sensing sensitivity and reduced operation time by eliminating the need for sample harvesting.[1] However, the on-site detection nature presents significant challenges to the sensitivity and durability of biomolecule detection due to the challenge of forming body-conformable electronic interfaces,[2] which stem from the fundamentally contradictory properties between rigid, non-stretchable biosensors and soft, deformable tissues.[3]

Existing efforts to develop body-conformable electronic interfaces generally focus on the structural design of flexible electronics,[4] the material design of stretchable conductors,[5] and the interface design of dry adhesives.[6] Despite their progress, these efforts face several inherent challenges that limit their practical deployment, such as induced mechanical irritation, decreased electrical conductivity, and unsuitability for wet surfaces.[2a] Specifically, body-conformable electronic interfaces based on the structural design of flexible electronics can reduce effective stiffness by patterning intrinsically stiff materials into desired structures. Despite structural designs enabling macroscopic flexibility, the material retains intrinsic stiffness at the microscopic level, limiting its full conformity to soft tissues or substrates. This localized stiffness constrains the device's conformability, particularly during prolonged contact, where rigid regions fail to adapt to natural surface deformations.[7] In contrast, stretchable conductors such as PEDOT: PSS hydrogels and liquid metals possess tissue-like softness, favorable for body-comfortable electronic interfaces.[5c,8] However, their electrical conductivities remain orders of magnitude lower than metallic conductors, limiting their electronic performance.

T. H. Wong, J. Liu, C. Anway, C. Ye, Z. Yu, S. Lin
Department of Mechanical Engineering
Michigan State University
East Lansing 48824, MI, USA
E-mail: linshaot@msu.edu

Y. Cheng, X. Liu
Department of Chemical Engineering and Materials Science
Michigan State University
East Lansing 48824, MI, USA
E-mail: xyliu@msu.edu

Y. Xie, Y. Wang
Department of Animal Science
Michigan State University
East Lansing 48824, MI, USA

R. Lu
College of Natural Science
Michigan State University
East Lansing 48824, MI, USA

The ORCID identification number(s) for the author(s) of this article can be found under https://doi.org/10.1002/aisy.202400697.

© 2024 The Author(s). Advanced Intelligent Systems published by Wiley-VCH GmbH. This is an open access article under the terms of the Creative Commons Attribution License, which permits use, distribution and reproduction in any medium, provided the original work is properly cited.

DOI: 10.1002/aisy.202400697

In addition to the structural design of flexible electronics and the material design of stretchable conductors, the adhesion between electronic components and tissue surfaces is crucial for stable and long-term body-conformable electronic interfaces. Various forms of dry adhesives have been developed owing to their reversibility and reusability.[9] However, because dry adhesives typically rely on physical interactions such as van de Waals, electrostatic forces, and friction,[10] they are generally ineffective on wet surfaces.

Hydrogels, polymer networks infiltrated with water, share similar mechanical and physiological properties as biological tissues, and have been regarded as an ideal material candidate to form long-term, high-efficacy, multi-modal interfaces between electronic components and biological systems.[11] In particular, the recent development of tissue-adhesive hydrogel patches have shown remarkable success in establishing rapid (<5 s) and robust adhesion (>400 J m^{-2}) between wet tissues and electronic devices for heart rate monitoring,[12] electrical stimulation,[13] electrophysiological recording,[14] and tissue imaging.[15] Although these efforts have not been implemented for in-situ biosensing, their success indicates the feasibility of tissue-adhesive hydrogel patch for interfacing rigid, non-stretchable biosensors with soft, deformable tissues.

Here, we develop an electrical tissue adhesive that can rapidly and robustly adhere electrochemical biosensors with biological tissues, enabling strain-insensitive physiological monitoring. The electrical tissue adhesive consists of two interpenetrating polymer networks: 1) an entangled adhesive polymer network that forms tough adhesions with both biological tissues and electrical components, and 2) a sacrificial dissipative polymer network that provides mechanical dissipation for enhanced toughness. The electrical tissue adhesive achieves a high fracture toughness of up to 3000 J m^{-2}, a low Young's modulus of around 20 kPa, and superior stretchability up to 15 times its initial length. When adhered between biosensors and tissues, its overall interfacial toughness reaches up to 500 J m^{-2}. Using an electrochemical glucose sensor as one example, we demonstrate that the electrical tissue adhesive can maintain resilient glucose sensing performance with less than 2% variation under various stress states and stretch levels. Using experiments and simulations, we show that the strain-insensitive biosensing performance is attributed to the high interfacial toughness and the superior compliance of the electrical tissue adhesive, which acts as a soft cushion effectively reducing stress concentration and retarding crack extension caused by the modulus mismatch between rigid biosensors and soft tissues. Additionally, we demonstrate its application for in-situ monitoring of exercise and diet in human subjects with various BMIs by measuring glucose concentration in sweat for 24 h. The development of electrical tissue adhesives represents an ideal platform to form long-term, high-efficacy, multi-modal interfaces between rigid, non-stretchable biosensors and soft, deformable tissues.

2. Results

2.1. Design of Electrical Tissue Adhesive

Figure 1a illustrates the primary application scenarios of the electrical tissue adhesive, which are categorized into external and internal sensing. These include, but are not limited to, the brain, stomach, intestines, and skin surface, where the electrical tissue adhesive enables in-situ real-time sensing and monitoring. Figure 1b schematically illustrates the working principle of the electrical tissue adhesive, serving as an interfacial layer forming robust covalent adhesions between rigid, nonstretchable biosensors and soft, deformable tissues. Specifically, the electrical tissue adhesive consists of two interpenetrating polymer networks (Figure 1c): 1) NHS-functionalized poly(acrylic acid) (PAAc-NHS) that forms the entangled adhesive polymer network, forming tough adhesions with both biological tissues and electrical components, and 2) gelatin that constitutes the sacrificial dissipative polymer network, providing mechanical dissipation for enhanced toughness. As the electrical tissue adhesive is subjected to tension, the long polymer chains within the entangled polymer network elongate and slide against each other, effectively distributing the stress without breaking.[16] Additionally, the inter- and intramolecular interactions within the gelatin network dissociate, providing substantial mechanical dissipations.[16b,17] Beyond its strong adhesion and high toughness, the electrical tissue adhesive also acts as a soft cushion, mitigating deformation of the biosensor caused by tissue movement while retarding interfacial crack extension at the interfaces between the rigid biosensor and soft tissues. Consequently, the superior mechanical compliance and high interfacial toughness ensure strain-insensitive biosensing performance, effectively mitigating motion artifacts from tissue movement (Figure 1d). For the biosensor, we adopt the electrochemical glucose biosensor as a representative example. To fabricate the sensing electrode, we first coat a layer of gold on top of a polyimide (PI) film. Next, we electroplate a thin layer of platinum nanoparticles (i.e., Pt black) onto the gold surface, followed by grafting a layer of glucose oxidase (GOx) onto it. Surrounding the sensing electrode, a circuit is formed with another electrode coated with a layer of silver/silver chloride (Ag/AgCl). This circuit generates electrical signals correlated with the concentration of glucose interacting with the glucose oxidase (Figure 1b). Details on the fabrication and functionalization of electrodes can be found in Figure S1 and S2, Supporting Information, respectively.

2.2. Dry-Crosslinking Mechanisms of Electrical Tissue Adhesive

The electrical tissue adhesive functions by covalently crosslinking to both biosensors and to wet tissues. To form robust adhesion with biosensors, we employ an amine-functionalized PI film as the supporting substrate, which readily forms strong covalent crosslinking with the NHS groups in the PAAc-NHS polymer network. To activate the covalent crosslinking, we apply a layer of water to the dry hydrogel film and gently press the biosensor onto the hydrogel film (Figure S3, Supporting Information). To form rapid and robust adhesion with wet tissues (i.e., porcine skin in this work), we adopt a dry-adhesion mechanism as reported in previous studies.[18] As illustrated in **Figure 2**a and Figure S4, Supporting Information, the adhesion process begins with a dry hydrogel film of controlled thickness T_h. The film is gently pressed onto a wet tissue surface for ≈5 s, and then left in an ambient environment for a controlled adhesion time t_a. During this time, the PAAc-NHS polymer network rapidly

© 2024 The Author(s). Advanced Intelligent Systems published by Wiley-VCH GmbH

26404567, 0, Downloaded from https://onlinelibrary.wiley.com/doi/10.1002/aisy.202400697 by Michigan State University, Wiley Online Library on [29/10/2024]. See the Terms and Conditions (https://onlinelibrary.wiley.com/terms-and-conditions) on Wiley Online Library for rules of use; OA articles are governed by the applicable Creative Commons License

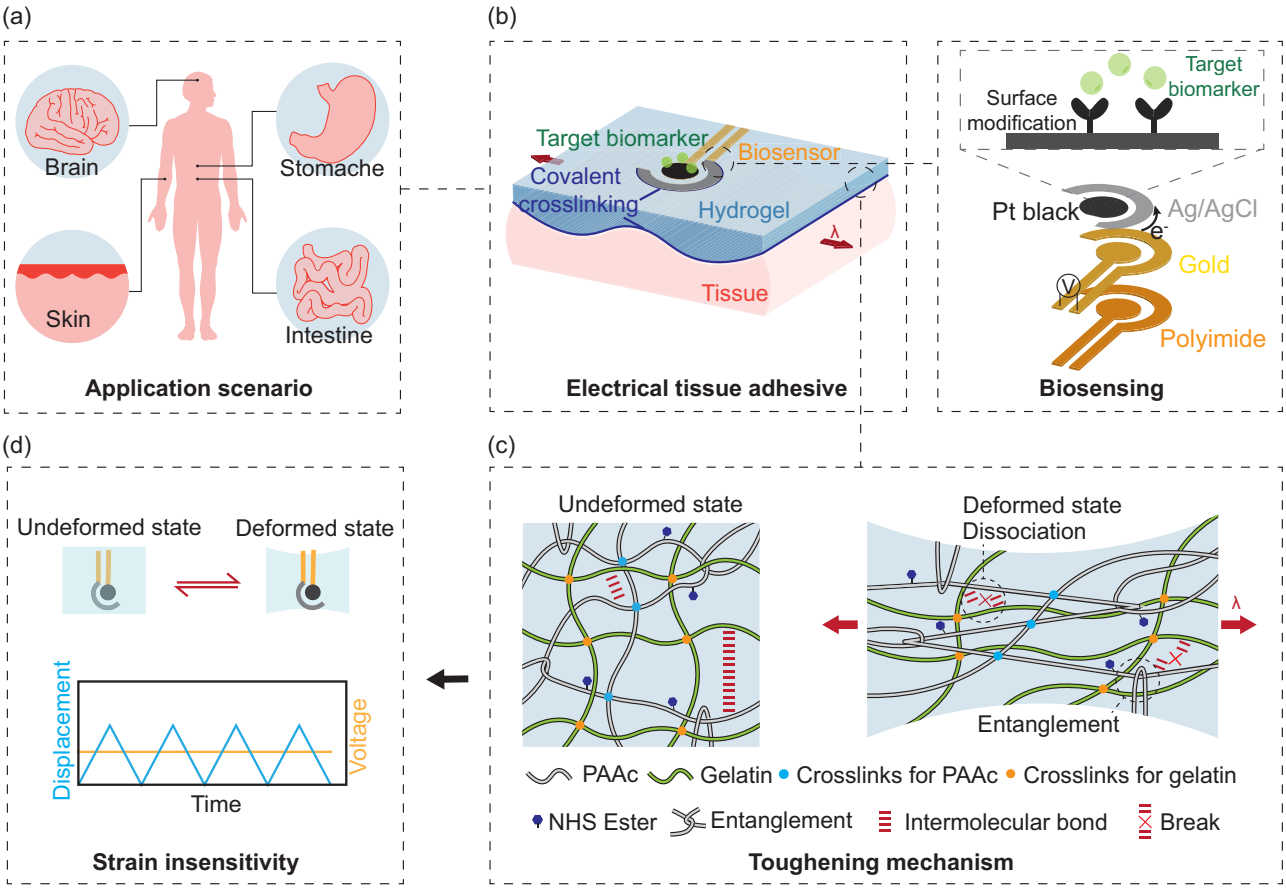


Figure 1. Design of electrical tissue adhesive. a) Primary application scenarios of the electrical tissue adhesive. b) The left schematic illustrates the electrical tissue adhesive, forming robust adhesion to rigid, nonstretchable biosensors and soft, deformable tissues. The electrical tissue adhesive enables strain-insensitive in-situ biosensing by mitigating the biosensor deformation caused by tissues, thanks to the superior mechanical compliance and high interfacial toughness of the electrical tissue adhesive. The right schematic illustrates the key components of the electrochemical glucose biosensor, including PI film, gold, Pt black, GOx, and Ag/AgCl. c) Schematics of the molecular structure of the electrical tissue adhesive, which consists of two interpenetrating polymer networks: 1) NHS-functionalized poly (acrylic acid) (PAAc-NHS) that forms the entangled adhesive polymer network, forming tough adhesions with both biological tissues and electrical components, and 2) gelatin that constitutes the sacrificial dissipative polymer network, providing mechanical dissipation for enhanced toughness. d) Strain insensitivity of the electrical tissue adhesive, attributed to superior mechanical compliance and high interfacial toughness of the electrical tissue adhesive.

transitions from a glassy to a rubbery state by absorbing water molecules from the tissue surface. The substantial negatively charged carboxylic acid groups in the PAAc-NHS polymer network enable rapid water absorption, facilitating covalent crosslinking between the NHS groups in the polymer network and the amine groups in the wet tissues (Figure S5, Supporting Information).

We first carry out T-peel tests to evaluate the effect of the adhesion time t_a on the interfacial toughness between the porcine skin and the PI film adhered by the dry adhesive film (Figure S6, Supporting Information). As shown in Figure 2b, for the dry adhesive film with a fixed thickness of 50 μm, the interfacial toughness initially increases from 54 to 444 J m^{-2} as the adhesion time t_a reaches 3 min, and then stabilizes at ≈520 J m^{-2} when the adhesion time t_a reaches 7 min. This finding indicates that the dry adhesive film requires a time duration to establish stable adhesion, which is physically determined by the time for water migration and the time for covalent crosslinking. We further carry out T-peel tests to evaluate the effect of the dry adhesive film thickness T_h on the interfacial toughness. The thickness of the dry adhesive film not only influences the rate of water migration from wet tissues to polymer networks but also determines the rigidity of the film that in turn affects the conformability of electrical tissue adhesive on tissue surfaces. As shown in Figure 2c, for the dry adhesive film attached to the wet tissue with a controlled adhesion time $t_a = 7$ min, the interfacial toughness decreases from 520 to 250 J m^{-2} as the thickness of the dry adhesive film T_h increases. This decrease can possibly be attributed to two factors: reduced conformability caused by the increased rigidity of the film and suppressed water absorption due to the retained glassy domains in the thicker dry adhesive film. We further measured the interfacial toughness of the electrical tissue adhesive exposed to ambient air for up to 24 min. As shown in Figure S7, Supporting Information, the interfacial toughness slightly increases despite the dehydration of the electrical tissue adhesive. We further measured the

© 2024 The Author(s). Advanced Intelligent Systems published by Wiley-VCH GmbH

26404567, 0, Downloaded from https://onlinelibrary.wiley.com/doi/10.1002/aisy.202400697 by Michigan State University, Wiley Online Library on [29/10/2024]. See the Terms and Conditions (https://onlinelibrary.wiley.com/terms-and-conditions) on Wiley Online Library for rules of use; OA articles are governed by the applicable Creative Commons License

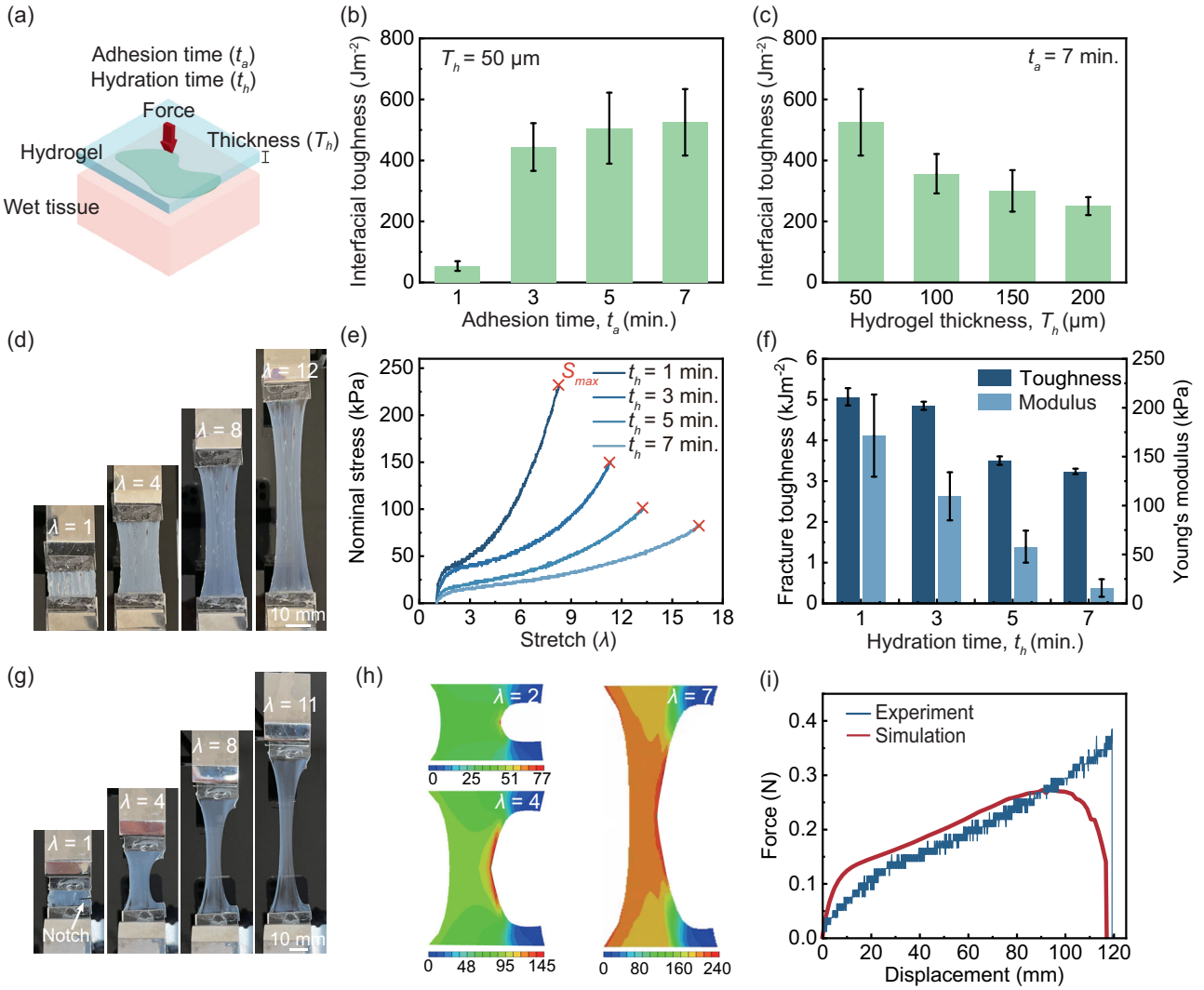


Figure 2. Interfacial and bulk characterizations of the electrical tissue adhesive. a) Schematic of the electrical tissue adhesive attaching onto a wet biological tissue, identifying three parameters, adhesion time (t_a), hydration time (t_h), and hydrogel thickness (T_h), that affect the interfacial and bulk properties. b) Interfacial toughess between the porcine skin and the PI film adhered by the dry adhesive film with a fixed thickness ($T_h = 50$ μm), at various adhesion time (t_h). c) Interfacial toughess between the porcine skin and the PI film adhered by the dry adhesive film with various thickness, at a fixed adhesion time ($t_a = 7$ min). d) Optical images of an unnotched electrical tissue adhesive under pure shear tensile test. e) Stress–stretch curves of the unnotched electrical tissue adhesives with various hydration times (t_h) under pure shear tensile test. f) Summarized fracture toughness and shear modulus of electrical tissue adhesives with various hydration times (t_h). g) Optical images of a notched electrical tissue adhesive under pure shear tensile test. h) Finite element simulation of crack propagation in a notched electrical tissue adhesive under pure shear tensile test. i) Comparison of force–displacement curves between experiment and simulation in a notched specimen under pure shear tensile test. Values in (b,c,f) represent the mean and the standard deviation (n = 3). Scale bars in (d,g) are 10 mm.

interfacial toughness of the electrical tissue adhesive immersed in a water bath, which slightly decreases possibly due to swelling-induced weakening of the electrical tissue adhesive (Figure S7, Supporting Information).

2.3. Toughening Mechanisms of Electrical Tissue Adhesive

Since the dry-adhesion mechanisms of the electrical tissue adhesive are intrinsically correlated with its hydration, we further investigate the effect of hydration time t_h on the bulk properties of the electrical tissue adhesive. We first characterize the swelling of the dry adhesive film as a function of hydration time. As shown in Figure S8, Supporting Information, the hydrogel thickness increases significantly as the hydration time extends up to 8 min and gradually reaches a steady-state value at ≈14 min. We observe that the steady-state hydration time (i.e., $t_h = 14$ min) for the dry adhesive film to reach its equilibrium state is longer than the steady-state adhesion time (i.e., $t_a = 7$ min) required for the film to achieve its maximum interfacial toughness. This is because the dry-adhesion process requires hydration only of the polymer network adjacent to the wet tissues, not the entire dry adhesive film. Therefore,

© 2024 The Author(s). Advanced Intelligent Systems published by Wiley-VCH GmbH

26404567, 0, Downloaded from https://onlinelibrary.wiley.com/doi/10.1002/aisy.202400697 by Michigan State University, Wiley Online Library on [29/10/2024]. See the Terms and Conditions (https://onlinelibrary.wiley.com/terms-and-conditions) on Wiley Online Library for rules of use; OA articles are governed by the applicable Creative Commons License

26404567, 0, Downloaded from https://onlinelibrary.wiley.com/doi/10.1002/aisy.202400697 by Michigan State University, Wiley Online Library on [29/10/2024]. See the Terms and Conditions (https://onlinelibrary.wiley.com/terms-and-conditions) on Wiley Online Library for rules of use; OA articles are governed by the applicable Creative Commons License

we characterize the bulk properties of the electrical tissue adhesive at various hydration times, up to 7 min. We first conduct pure shear tensile tests on unnotched specimens to measure the nominal stress versus stretch curves of electrical tissue adhesives at different hydration times (Figure 2d). As shown in Figure 2e, the electrical tissue adhesive with a hydration time $t_h = 1$ min exhibits a high strength of 227 kPa, and a stretchability of 8.3. In contrast, with a hydration time $t_h = 7$ min, its strength decreases to 83.5 kPa, while its stretchability increases to 16.6. Additionally, as the hydration time increases, Young's modulus of the electrical tissue adhesive significantly decreases from 171.5 to 17.5 kPa (Figure 2f). We further conduct pure shear tensile tests on notched specimens to measure the fracture toughness of electrical tissue adhesives at different hydration times (Figure 2g and Figure S9, Supporting Information). As summarized in Figure 2f, the fracture toughness of the electrical tissue adhesive decreases slightly from 5 to 3.2 k J m^{-2} as the hydration time increases from 1 to 7 min. Different from the significant reduction in Young's modulus due to hydration, the reduction of fracture toughness is moderate, which is mainly due to the competing effects caused by hydration: reduced density and increased length of bridging polymer chains at the crack tip.[16b,19]

To further uncover the toughening mechanisms of electrical tissue adhesive, we perform finite element simulation (FEA) to simulate crack propagation in the material, which accounts for the toughening contributions from both the entangled adhesive polymer network and the sacrificial dissipative polymer network. We use the Ogden model to simulate the nonlinear large deformation of the entangled adhesive polymer network (Figure S10a, Supporting Information), the Mullins-effect model to capture the hysteretic dissipation by the sacrificial dissipative polymer network (Figure S10b,c, Supporting Information), and the cohesive zone model to define the failure at the crack tip. Specifically, to extract the parameters of the Ogden model, we measure the nominal stress versus stretch curve of the electrical tissue adhesive after it has been subjected to cyclic tensile stress at a stretch ratio of 11 for 1000 cycles. Notably, the electrical tissue adhesive exhibits a negligible stress–stretch hysteresis ratio after 1000 cycles of loading (Figure S11, Supporting Information), indicating the low-hysteresis nature of the entangled adhesive polymer network. This observation is consistent with recent studies on entangled polymer networks.[16a,b] To extract the parameters of the Mullins-effect model, we perform cyclic loading on the electrical tissue adhesive at different stretch ratios (Figure S10b, Supporting Information) and summarize the hysteresis ratio as a function of stretch ratios (Figure S10c, Supporting Information). To extract the parameters of the cohesive zone model, we take the measured strength as the maximum stress and the fracture toughness of the entangled adhesive polymer network as the enclosed area of the traction–separation relationship in the model (Figure S12, Supporting Information). As shown in Figure 2h and Figure S13, Supporting Information, our simulation can capture the large deformation and crack blunting as observed in the fracture experiment (Figure 2g). Furthermore, the force versus stretch curve in simulation closely matches the experimental curve (Figure 2i), indicating that the toughening of the electrical tissue adhesive is due to the combined contributions of the entangled adhesive polymer network that exhibits negligible mechanical hysteresis and the sacrificial dissipative polymer network that exhibits large mechanical hysteresis.

2.4. Strain-Insensitive Mechanism of Electrical Tissue Adhesive

One key challenge faced by existing in-situ biosensors is performance variations caused by mechanical strain from the movement of wet tissues. The tissue movement inevitably alters the electrode geometry, leading to significant fluctuations in sensor performance.[7b,20] Here, we demonstrate that the electrical tissue adhesive (**Figure 3**a), acting as a soft cushion, effectively mitigates the deformation of the biosensor caused by tissue movement, enabling strain-insensitive biosensing. Additionally, the adhesions among electrical tissue adhesive, biosensors, and wet tissues must be strong enough to prevent performance variations caused by strain-induced delamination at the interfaces. We first perform finite element simulations to quantify the role of electrical tissue adhesive in mitigating the deformation of the electrode (Figure S14 and Movie S1, Supporting Information). As shown in Figure S14, Supporting Information, when the far field applied stretch ratio increases to 2, the strain of the electrical tissue adhesive adjacent to the electrode significantly rises to 0.8, while the strain of the electrode remains as low as 0.05. To further explore the role of electrical tissue adhesive in retarding crack extension, we simulate the detachment of the electrodes from tissue via physical attachment and electrical tissue adhesive (Figure 3c and Movie S2, Supporting Information). Specifically, we calculate the energy release rate at the electrode-tissue interface without electrical tissue adhesive and the energy release rates at the electrode–hydrogel and hydrogel–tissue interfaces with electrical tissue adhesive (Figure 3f). The results show that for the electrode relying on physical attachment, as the strain increases to 50%, the energy release rate is ≈17 J m^{-2}, significantly exceeding the toughness provided by physical attachment (assumed to be 1 J m^{-2}) (Figure 3d). In contrast, under the adhesion provided by the electrical tissue adhesive, the energy release rates at both the hydrogel–electrode and hydrogel–tissue interfaces are only 1.2 J m^{-2}, far below the interfacial toughness offered by the electrical tissue adhesive (≈500 J m^{-2}) (Figure 3g).

We further use experiments to assess the strain sensitivity of a gold electrode's electrical conductivity when the electrical tissue adhesive is subjected to controlled stress conditions. As shown in Figure 3e, the gold electrode does not experience observable detachment or damage as the electrical tissue adhesive is subjected to stretching, twisting, and bending. To quantify the impact of strain, we further measure the change in the gold electrode's electrical conductivity, which shows less than 2% variation throughout the stretching, twisting, and bending deformations (Figure 3h). The electrical hysteresis of the electrical tissue adhesive by monitoring the real-time resistance changes during a stretch cycle ($\lambda = 2$) is then measured (Figure S15, Supporting Information). The results show minimal resistance variation (less than 1%) throughout the loading and unloading process, confirming the adhesive's role as a soft cushion for the electrode, which can effectively maintain the electrode's structural stability during deformation.

© 2024 The Author(s). Advanced Intelligent Systems published by Wiley-VCH GmbH

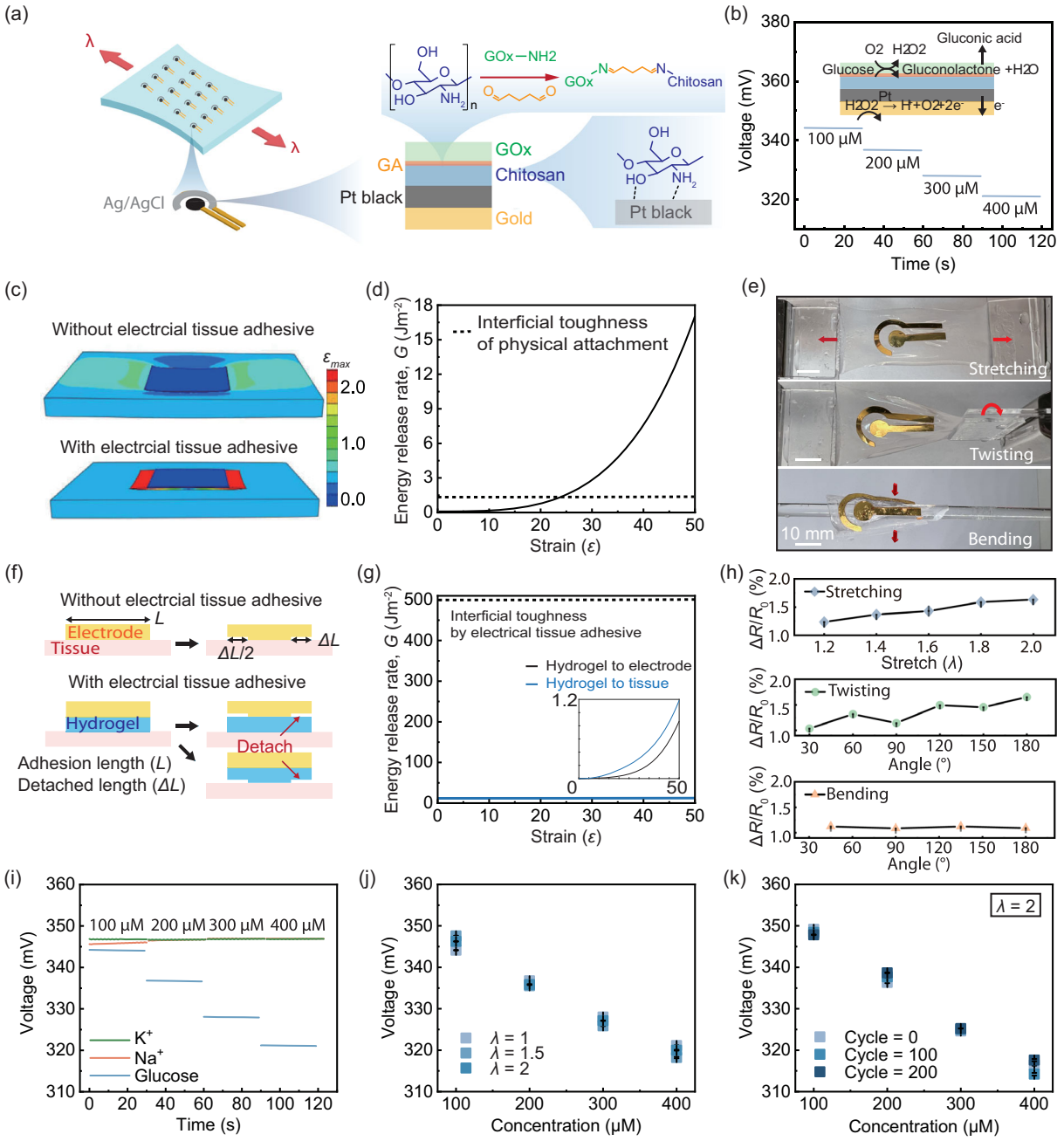


Figure 3. Strain–sensitivity characterization of electrical tissue adhesive for electrochemical glucose sensing. a) The left plot illustrates an array of electrochemical glucose sensors attached to the electrical tissue adhesive subjected to strain. The right plot illustrates the immobilization process of the electrochemical glucose sensor. b) The output voltage as a function of time corresponding to various glucose concentrations. The schematic illustrates the sensing mechanism of electrochemical glucose sensor. c) Strain distribution of strain distributions in skin tissue adhered to a gold electrode with and without electrical tissue adhesives under tension. d) Energy release rate of the electrode detaching from the tissue without electrical tissue adhesive, compared to the interfacial toughness of electrode physically attaching to tissue. e) Optical images of the electrical tissue adhesive adhered with gold electrode under stretching, twisting, and bending. f) Schematics illustrating electrode detachment from tissue with and without an electrical tissue adhesive. g) Energy release rate of the electrode detaching from tissue with electrical tissue adhesive (detachment occurring at either the hydrogel–tissue or hydrogel–electrode interfaces), compared to the interfacial toughness of the electrical tissue adhesive. h) The variation in the gold electrode's electrical conductivity $\Delta R/R_0$ as a function of applied stretch ratios, twisting angles, and bending angles on the electrical tissue adhesive, where ΔR represents the change in the gold electrode's electrical conductivity, and R_0 denotes the gold electrode's electrical conductivity in its undeformed state. i) Electrical responses of the electrochemical glucose sensor when detecting varying concentrations of K^+ ions, Na^+ ions, and glucose. j) Sensing performance of the electrochemical glucose sensor adhered to electrical tissue adhesive under various stretch conditions. k) Sensing performance of the electrochemical glucose sensor adhered to electrical tissue adhesive under different cycle numbers. Values in (h,j,k) represent the mean and the standard deviation (n = 5). Scale bars in (e) are 10 mm.

© 2024 The Author(s). Advanced Intelligent Systems published by Wiley-VCH GmbH

26404567, 0, Downloaded from https://onlinelibrary.wiley.com/doi/10.1002/aisy.202400697 by Michigan State University, Wiley Online Library on [29/10/2024]. See the Terms and Conditions (https://onlinelibrary.wiley.com/terms-and-conditions) on Wiley Online Library for rules of use; OA articles are governed by the applicable Creative Commons License

The frequency of deformation is another key factor for ensuring sensing stability. While electrochemical sensors are typically designed for low-frequency signal collection, such as monitoring biomarker concentrations in physiological fluids, we assess the performance of electrical tissue adhesive under dynamic loading such as that in dynamic organs. As shown in Figure S16, Supporting Information, the loading frequency has a negligible effect on electrical resistance variation, ensuring stable sensing performance under dynamic loading with frequency ranging from 0.1 to 0.5 Hz. We also measure the variation of electrical resistance when the electrical tissue adhesive is subjected to cyclic stretch up to different stretches. As shown in Figure S17, Supporting Information, the change in electrical conductivity remains less than 1% throughout the cycle loading. Note that the electrical measurements of the electrical tissue adhesive are performed after a 48-hour immersion in phosphate-buffered saline (PBS).

Using electrochemical glucose sensing as one example, we next evaluate the strain sensitivity of glucose sensing by subjecting the electrical tissue adhesive to controlled stretch ratios and cycle numbers. To fabricate the sensing electrode of the electrochemical glucose biosensor, we first electroplate Pt black onto the gold electrode (Figure 3a). Chitosan is then physically immobilized onto the Pt black,[21] followed by the bonding of the glucose oxidase enzyme (GOx), which is crosslinked by glutaraldehyde (GA).[22] Surrounding the sensing electrode, a circuit is formed with another electrode (i.e., reference electrode) coated with a layer of silver/silver chloride (Ag/AgCl). This circuit generates electrical signals, which are correlated with the concentration of glucose interacting with glucose oxidase. Specifically, glucose is first oxidized to gluconolactone and hydrogen peroxide (H_2O_2) by GOx, and subsequently converted into gluconic acid. The platinum nanoparticles on the electrode then reduce the generated H_2O_2, releasing electrons and generating an electrical signal from the flow of these electrons. We first calibrate the glucose sensing performance with the electrical tissue adhesive in its undeformed state. As shown in Figure 3b, the output voltage of the glucose sensor is inversely proportional to the glucose concentration, with ≈345 mV at 100 μM, 315 mV at 400 μM, and a determination coefficient (R^2) of 0.989. We also demonstrate that the glucose sensing performance is negligibly impacted by mobile ions such as potassium ions (K^+) and sodium ions (Na^+), which are ubiquitously present in body fluid, thereby highlighting its specificity for detecting glucose (Figure 3i). We next assess the glucose sensing performance of the electrical tissue adhesive at its deformed state. As shown in Figure 3j and Figure S18a, Supporting Information, the electrochemical glucose biosensor maintains stable sensing performance even when the electrical tissue adhesive is subjected to controlled stretch ratios up to 2. Furthermore, the biosensor exhibits negligible sensing variation when the electrical tissue adhesive undergoes repeated cyclic loading up to 200 cycles (Figure 3k and Figure S18b, Supporting Information).

2.5. Demonstration of Electrical Tissue Adhesive for In-situ Monitoring of Exercise and Diet

Next, we demonstrate the application of electrical tissue adhesive for in-situ monitoring of exercise and diet in human subjects by measuring glucose concentration in sweat. We first characterize the biocompatibility of the electrical tissue adhesive (Figure S19, Supporting Information). The experimental results demonstrate excellent biocompatibility, with cell viability after 24 h of incubation showing no significant difference from the positive control, both exhibiting cell viability above 97%. This confirms that the electrical tissue adhesive is biologically safe for interaction with biological tissues. **Figure 4**a schematically illustrates the working principle. When the electrical tissue adhesive is physically attached to sweat-covered skin, a portion of the sweat is rapidly absorbed by the dry hydrogel adhesive film, facilitating tissue adhesion through covalent crosslinking. Simultaneously, the electrochemical glucose biosensor interacts with the sweat, generating electrical signals corresponding to the glucose concentration. We examine two scenarios affecting glucose concentration in the human body: exercise and diet. During prolonged exercise without adequate hydration, glucose levels in the body decrease. Conversely, after a night of fasting, glucose levels drop due to extended fasting and return to normal levels after food intake. By comparing data before and after these scenarios, we can monitor the status of subjects through in-situ monitoring of glucose concentrations in human sweat.

Figure 4b shows the electrical tissue adhesive with the electrochemical glucose biosensor before application and after conformally attaching it to human skin. Despite the extruding, stretching, and twisting of the skin, there is no observable plastic deformation of the electrical tissue adhesive or surface detachment at the interface. This demonstrates that the electrical tissue adhesive effectively protects the underlying glucose biosensor, providing a stable foundation for subsequent testing. We then test the adhesion duration of the electrical tissue adhesive on the skin and its long-term capability to detect glucose concentrations in sweat. As shown in Figure 4c, the electrical tissue adhesive maintains its adherence to the skin, providing a stable detection platform for the biosensor over 24 h. Additionally, we conduct further experiments extending up to 48 h (Figure S20, Supporting Information). We next tested the glucose concentrations in the sweat of three human subjects with different body mass indices (BMI) before and after exercise and diet. As shown in Figure 4d, subject 1's glucose concentration noticeably decreases from ≈120 to 80 μM after 30 min of exercise. Conversely, after food intake, the concentration increases from 110 to ≈140 μM. These findings indicate that the glucose sensor effectively reflects glucose concentrations in the subject's sweat. Moreover, with the electrical tissue adhesive, the sensor remains reliably attached to the skin during exercise and meals, enabling convenient subsequent detections. Similar trends in glucose concentration variation during exercise and meals are observed for the other two human subjects (Figure 4e). Notably, subject 1, with a higher body mass index (BMI), shows an overall higher concentration than human subjects 2 and 3. These findings validate the effectiveness of our glucose biosensor in detecting human glucose concentrations, especially when paired with the electrical tissue adhesive for reliable adhesion. Through experiments and simulations, we conclude that the electrical tissue adhesive provides stable adhesion to tissues for sensors, minimally unaffected by external factors, including deformation and frequency. Based on this stable adhesion platform, the adhesive holds significant potential for a wide range of applications,

© 2024 The Author(s). Advanced Intelligent Systems published by Wiley-VCH GmbH

26404567, 0, Downloaded from https://onlinelibrary.wiley.com/doi/10.1002/aisy.202400697 by Michigan State University, Wiley Online Library on [29/10/2024]. See the Terms and Conditions (https://onlinelibrary.wiley.com/terms-and-conditions) on Wiley Online Library for rules of use; OA articles are governed by the applicable Creative Commons License

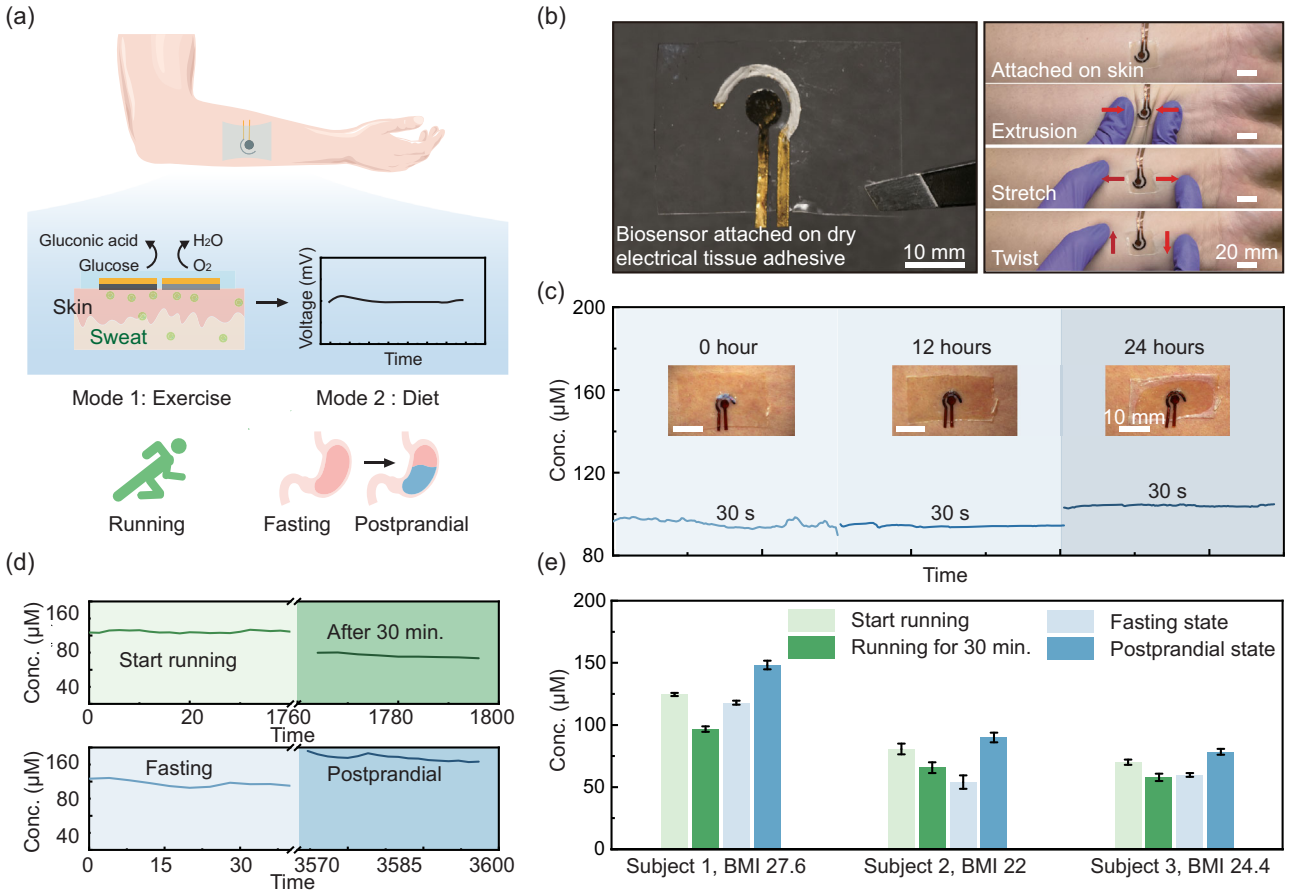


Figure 4. Demonstration of electrical tissue adhesive for monitoring of daily activities. a) Schematic of an electrical tissue adhesive applied to the skin for sensing glucose concentration in sweat, monitoring changes in concentration throughout exercise and dietary intake. b) Optical images of an electrical tissue adhesive attached to the skin (left) and undergoing various deformations (right). c) Long-term monitoring of the glucose concentration over 24 h with corresponding optical images at various intervals. d) Real-time sensing of glucose concentration before and after running (top), fasting and postprandial (bottom) of human subject 1. e) Measured glucose concentration before and after running for exercise monitoring, and during fasting and postprandial states for dieting monitoring in three human subjects with different BMIs. Values in (e) represent the mean and the standard deviation ($n = 5$). Scale bars in (b left) and (b right) are 10 and 20 mm, respectively.

independent of the type of sensor (here, we demonstrate glucose and lactate sensors as examples (Figure S21, Supporting Information)). Additionally, we have supplemented data on long-term adhesion performance and strain-insensitivity under PBS immersion, further validating its potential for in vivo applications.

3. Discussion

A key challenge for in-situ biosensors is ensuring long-term adhesion between the sensor and skin tissue, where this difficulty arises from the dynamic nature of biological tissues and the modulus mismatch between the electrodes and the skin. In this work, we introduce a strategy that applies hydrogels as the adhesive material between biological tissues and biosensors. As polymer networks infiltrated with water, hydrogels have similar mechanical and physiological properties as biological tissues, and are regarded as one of the most dedicated material candidates to form long-term, high-efficacy, multi-modal interfaces between electronic components and biological systems. We demonstrate a hydrogel-based electrical tissue adhesive forming instantaneous adhesion to both biosensors and wet tissues and reaching an overall interfacial toughness of 500 J m^{-2}. We identify three parameters that critically affect the adhesion and bulk properties of the electrical tissue adhesive: 1) hydrogel thickness, 2) adhesion time, and 3) hydration time. Using electrochemical glucose biosensing as one example, we demonstrate the electrical tissue adhesive effectively minimizes sensing performance variations due to strain, thanks to the superior mechanical compliance and high interfacial toughness of the electrical tissue adhesive. Such strain-insensitive sensing performance ensures minimal impact from surrounding skin movement during practical operations, such as long-term and stable monitoring of daily activities by in-situ measuring glucose concentration in human sweat. Compared to recently reported skin-adhesive electronic devices, our device demonstrates superior adhesion performance and strain insensitivity (Table S1, Supporting Information).

© 2024 The Author(s). Advanced Intelligent Systems published by Wiley-VCH GmbH

26404567, 0, Downloaded from https://onlinelibrary.wiley.com/doi/10.1002/aisy.202400697 by Michigan State University, Wiley Online Library on [29/10/2024]. See the Terms and Conditions (https://onlinelibrary.wiley.com/terms-and-conditions) on Wiley Online Library for rules of use; OA articles are governed by the applicable Creative Commons License

This work not only provides a first-of-its-kind strategy for creating body-comfortable electronic interfaces between rigid, non-stretchable biosensors and soft, deformable tissues but also potentially offers a multi-model platform for in-situ biosensing and site-specific delivery, revolutionizing the field of medicine through real-time monitoring, personalized diagnosis, and targeted therapies.

Supporting Information

Supporting Information is available from the Wiley Online Library or from the author.

Acknowledgements

We acknowledge the funding support from the National Science Foundation (CBET-2320716) and National Science Foundation (CMMI-2338747).We acknowledge Claudia Chen for assisting the fabrication of the sensing electrodes. Tests on human skin performed at Michigan State University were approved by the Institutional Review Board (IRB), Michigan State University, and informed written consent was obtained (approval number: STUDY00011110).

Conflict of Interest

The authors declare no conflict of interest.

Author Contributions

Tsz Hung Wong: Conceptualization (lead); Data curation (lead); Formal analysis (lead); Methodology (lead); Validation (lead); Visualization (lead); Writing—original draft (lead). **Jiabin Liu**: Data curation (supporting); Formal analysis (supporting); Investigation (supporting); Methodology (supporting). **Yijie Cheng**: Data curation (supporting); Formal analysis (supporting); Methodology (supporting); Writing—review and editing (supporting). **Yilin Xie**: Data curation (supporting); Formal analysis (supporting); Methodology (supporting); Resources (supporting); Writing—review and editing (supporting). **Camryn Anway**: Data curation (supporting); Formal analysis (supporting). **Ruihao Lu**: Data curation (supporting); Formal analysis (supporting). **Chuwei Ye**: Data curation (supporting); Formal analysis (supporting). **Zhaohan Yu**: Data curation (supporting); Formal analysis (supporting). **Yuan Wang**: Resources (supporting); Supervision (supporting); Writing—review and editing (supporting). **Xinyue Liu**: Formal analysis (equal); Funding acquisition (equal); Investigation (equal); Supervision (equal); Writing—review and editing (equal). **Shaoting Lin**: Conceptualization (lead); Funding acquisition (lead); Investigation (lead); Methodology (lead); Project administration (lead); Supervision (lead); Validation (lead); Writing—review and editing (lead).

Data Availability Statement

The data that support the findings of this study are available from the corresponding author upon reasonable request.

Keywords

in-situ biosensing, tissue adhesives, tough hydrogels

Received: August 12, 2024
Revised: October 1, 2024
Published online:

[1] a) W. Gao, S. Emaminejad, H. Y. Y. Nyein, S. Challa, K. Chen, A. Peck, H. M. Fahad, H. Ota, H. Shiraki, D. Kiriya, *Nature* **2016**, *529*, 509; b) E. De la Paz, N. H. Maganti, A. Trifonov, I. Jeerapan, K. Mahato, L. Yin, T. Sonsa-Ard, N. Ma, W. Jung, R. Burns, *Nat. Commun.* **2022**, *13*, 7405; c) Y. Song, J. Min, Y. Yu, H. Wang, Y. Yang, H. Zhang, W. Gao, *Sci. Adv.* **2020**, *6*, eaay9842; d) H. Park, W. Park, C. H. Lee, *NPG Asia Mater.* **2021**, *13*, 23.

[2] a) S. Liu, Y. Rao, H. Jang, P. Tan, N. Lu, *Matter* **2022**, *5*, 1104; b) D.-H. Kim, N. Lu, R. Ma, Y.-S. Kim, R.-H. Kim, S. Wang, J. Wu, S. M. Won, H. Tao, A. Islam, *Sci. Adv.* **2011**, *333*, 838.

[3] a) X. Liu, J. Liu, S. Lin, X. Zhao, *Mater. Today* **2020**, *36*, 102; b) J. Zhang, L. Wang, Y. Xue, I. M. Lei, X. Chen, P. Zhang, C. Cai, X. Liang, Y. Lu, J. Liu, *Adv. Mater.* **2023**, *35*, 2209324; c) S. Lin, H. Yuk, T. Zhang, G. A. Parada, H. Koo, C. Yu, X. Zhao, *Adv. Mater.* **2016**, *28*, 4497.

[4] a) N. Lu, *Soft Robot.* **2014**, *1*, 53; b) Y. Sun, J. A. Rogers, *Adv. Mater.* **2007**, *19*, 1897.

[5] a) Y. Liu, J. Liu, S. Chen, T. Lei, Y. Kim, S. Niu, H. Wang, X. Wang, A. M. Foudeh, J. B.-H. Tok, *Nat. Biomed. Eng.* **2019**, *3*, 58; b) S. Wang, J. Xu, W. Wang, G.-J. N. Wang, R. Rastak, F. Molina-Lopez, J. W. Chung, S. Niu, V. R. Feig, J. Lopez, *Nature* **2018**, *555*, 83; c) B. Lu, H. Yuk, S. Lin, N. Jian, K. Qu, J. Xu, X. Zhao, *Nat. Commun.* **2019**, *10*, 1043; d) H.-J. Kim, K. Sim, A. Thukral, C. Yu, *Sci. Adv.* **2017**, *3*, e1701114; e) K. Sim, Z. Rao, H.-J. Kim, A. Thukral, H. Shim, C. Yu, *Sci. Adv.* **2019**, *5*, eaav5749.

[6] a) L. Ding, C. Hang, S. Yang, J. Qi, R. Dong, Y. Zhang, H. Sun, X. Jiang, *Nano Lett.* **2022**, *22*, 4482; b) D. W. Kim, M. Kong, U. Jeong, *Adv. Sci.* **2021**, *8*, 2004170; c) M. K. Kwak, C. Pang, H. E. Jeong, H. N. Kim, H. Yoon, H. S. Jung, K. Y. Suh, *Adv. Funct. Mater.* **2011**, *21*, 3606.

[7] a) Y. Zhao, B. Wang, J. Tan, H. Yin, R. Huang, J. Zhu, S. Lin, Y. Zhou, D. Jelinek, Z. Sun, *Science* **2022**, *378*, 1222; b) W. Wang, S. Wang, R. Rastak, Y. Ochiai, S. Niu, Y. Jiang, P. K. Arunachala, Y. Zheng, J. Xu, N. Matsuhisa, X. Yan, S. Kwon, M. Miyakawa, Z. Zhang, R. Ning, A. Foudeh, Y. Yun, C. Linder, J. B.-H. Tok, Z. Bao, *Nat. Electron.* **2021**, *4*, 143; c) H. Li, P. Tan, Y. Rao, S. Bhattacharya, Z. Wang, S. Kim, S. Gangopadhyay, H. Shi, M. Jankovic, H. J. C. R. Huh, *Chem. Rev.* **2024**, *124*, 3220.

[8] a) A. Inoue, H. Yuk, B. Lu, X. Zhao, *Sci. Adv.* **2020**, *6*, eaay5394; b) H. Yuk, B. Lu, S. Lin, K. Qu, J. Xu, J. Luo, X. Zhao, *Nat. Commun.* **2020**, *11*, 1604.

[9] a) T. Kim, J. Park, J. Sohn, D. Cho, S. Jeon, *ACS nano* **2016**, *10*, 4770; b) S. Wang, Y. Fang, H. He, L. Zhang, C. A. Li, J. Ouyang, *Adv. Funct. Mater.* **2021**, *31*, 2007495; c) S. Baik, D. W. Kim, Y. Park, T.-J. Lee, S. Ho Bhang, C. Pang, *Nature* **2017**, *546*, 396.

[10] a) S. Chun, D. W. Kim, S. Baik, H. J. Lee, J. H. Lee, S. H. Bhang, C. Pang, *Adv. Funct. Mater.* **2018**, *28*, 1805224; b) S. Baik, H. J. Lee, D. W. Kim, J. W. Kim, Y. Lee, C. Pang, *Adv. Mater.* **2019**, *31*, 1803309.

[11] a) H. Yuk, B. Lu, X. Zhao, *Chem. Soc. Rev.* **2019**, *48*, 1642; b) S. Li, Y. Cong, J. Fu, *J. Mater. Chemi. B* **2021**, *9*, 4423; c) Q. Yang, Z. Hu, J. A. Rogers, *Acc. Mater. Res.* **2021**, *2*, 1010.

[12] a) H. Lei, J. Zhao, X. Ma, H. Li, D. Fan, *Adv. Healthcare Mater.* **2021**, *10*, 2101089; b) J. Zhang, S. Shen, R. Lin, J. Huang, C. Pu, P. Chen, Q. Duan, X. You, C. Xu, B. Yan, *Adv. Mater.* **2023**, *35*, 2209497.

[13] a) L. Mao, S. Hu, Y. Gao, L. Wang, W. Zhao, L. Fu, H. Cheng, L. Xia, S. Xie, W. Ye, *Adv. Healthcare Mater.* **2020**, *9*, 2000872; b) C. Cai,

© 2024 The Author(s). Advanced Intelligent Systems published by Wiley-VCH GmbH

26404567, 0, Downloaded from https://onlinelibrary.wiley.com/doi/10.1002/aisy.202400697 by Michigan State University, Wiley Online Library on [29/10/2024]. See the Terms and Conditions (https://onlinelibrary.wiley.com/terms-and-conditions) on Wiley Online Library for rules of use; OA articles are governed by the applicable Creative Commons License

H. Zhu, Y. Chen, C. Chen, H. Li, Z. Yang, H. Liu, *Appl. Mater. Today* **2022**, *27*, 101491; c) G. Tian, D. Yang, C. Liang, Y. Liu, J. Chen, Q. Zhao, S. Tang, J. Huang, P. Xu, Z. Liu, *Adv. Mater.* **2023**, *35*, 2212302.

[14] a) C. Wang, S. S. Rubakhin, M. J. Enright, J. V. Sweedler, R. G. Nuzzo, *Adv. Funct. Mater.* **2021**, *31*, 2010246; b) F. Wang, Y. Xue, X. Chen, P. Zhang, L. Shan, Q. Duan, J. Xing, Y. Lan, B. Lu, J. Liu, *Adv. Funct. Mater.* **2023**, 2314471; c) R. Liu, T. Wang, G. Li, Z. Fan, Q. Zhou, K. Wang, P. Li, W. Huang, *Adv. Funct. Mater.* **2023**, *33*, 2214917; d) Y. Liu, C. Wang, J. Xue, G. Huang, S. Zheng, K. Zhao, J. Huang, Y. Wang, Y. Zhang, T. Yin, *Adv. Healthcare Mater.* **2022**, *11*, 2200653.

[15] a) C. Wang, X. Chen, L. Wang, M. Makihata, H.-C. Liu, T. Zhou, X. Zhao, *Science* **2022**, *377*, 517; b) H.-C. Liu, Y. Zeng, C. Gong, X. Chen, P. Kijanka, J. Zhang, Y. Genyk, H. Tchelepi, C. Wang, Q. Zhou, *Sci. Adv.* **2024**, *10*, eadk8426.

[16] a) D. Zheng, S. Lin, J. Ni, X. Zhao, *Extreme Mech. Lett.* **2022**, *51*, 101608; b) S. Lin, C. D. Londono, D. Zheng, X. Zhao, *Soft Matter* **2022**, *18*, 5742; c) J. Kim, G. Zhang, M. Shi, Z. Suo, *Sci. Adv.* **2021**, *374*, 212; d) M. Shi, J. Kim, G. Nian, Z. Suo, *Extreme Mech. Lett.* **2023**, *59*, 101953.

[17] a) Z. Wang, C. Xiang, X. Yao, P. Le Floch, J. Mendez, Z. Suo, *Proc. Natl. Acad. Sci. U.S.A.* **2019**, *116*, 5967; b) S. Lin, Y. Zhou, X. Zhao, *Extreme Mech. Lett.* **2014**, *1*, 70.

[18] H. Yuk, C. E. Varela, C. S. Nabzdyk, X. Mao, R. F. Padera, E. T. Roche, X. Zhao, *Nature* **2019**, *575*, 169.

[19] T. Zhang, S. Lin, H. Yuk, X. Zhao, *Extreme Mech. Lett.* **2015**, *4*, 1.

[20] a) J. Lee, S. J. Ihle, G. S. Pellegrino, H. Kim, J. Yea, C.-Y. Jeon, H.-C. Son, C. Jin, D. Eberli, F. Schmid, *Nat. Electron.* **2021**, *4*, 291; b) A. Abramson, C. T. Chan, Y. Khan, A. Mermin-Bunnell, N. Matsuhisa, R. Fong, R. Shad, W. Hiesinger, P. Mallick, S. S. Gambhir, *Sci. Adv.* **2022**, *8*, eabn6550; c) Q. Su, Q. Zou, Y. Li, Y. Chen, S.-Y. Teng, J. T. Kelleher, R. Nith, P. Cheng, N. Li, W. Liu, *Sci. Adv.* **2021**, *7*, eabi4563.

[21] S. F. Hamzavi, S. Jamili, M. Yousefzadi, A. Mashinchian Moradi, N. Amrollahi Biuki, *Mol. Divers.* **2020**, *24*, 985.

[22] A. Chmayssem, I. Shalayel, S. Marinesco, A. Zebda, *Sensors* **2023**, *23*, 465.

© 2024 The Author(s). Advanced Intelligent Systems published by Wiley-VCH GmbH

26404567, 0, Downloaded from https://onlinelibrary.wiley.com/doi/10.1002/aisy.202400697 by Michigan State University, Wiley Online Library on [29/10/2024]. See the Terms and Conditions (https://onlinelibrary.wiley.com/terms-and-conditions) on Wiley Online Library for rules of use; OA articles are governed by the applicable Creative Commons License